

---

# Visualization of Coherent Structures in Transient 2D Flows

Christoph Garth<sup>1</sup>, Guo-Shi Li<sup>2</sup>, Xavier Tricoche<sup>2</sup>, Charles D. Hansen<sup>2</sup>, and Hans Hagen<sup>1</sup>

<sup>1</sup> University of Kaiserslautern `garth|hagen@rhrk.uni-kl.de`

<sup>2</sup> University of Utah `lig|tricoche|hansen@sci.utah.edu`

## 1 Introduction

The depiction of a time-dependent flow in a way that effectively supports the structural analysis of its salient patterns is still a challenging problem for flow visualization research. While a variety of powerful approaches have been investigated for over a decade now, none of them so far has been able to yield representations that effectively combine good visual quality and a physical interpretation that is both intuitive and reliable. Yet, with the huge amount of flow data generated by numerical computations of growing size and complexity, scientists and engineers are faced with a daunting analysis task in which the ability to identify, extract, and display the most meaningful information contained in the data is becoming absolutely indispensable.

Arguably the major hurdle that hampers the effort of visualization researchers in the post-processing of transient flows is the difficulty to identify proper defining criteria for the coherency of the structures that these flows exhibit. Eulerian approaches focus on the patterns exhibited by streamlines at each instant of time and lend themselves to a topological classification of the flow features. While this leads to visualization algorithms that are computationally efficient and benefit from a strong theoretical framework, the connection of the corresponding structures to the physics of the flow remains unclear. The Lagrangian perspective on the other hand offers a more intuitive account of the material advection induced by the flow but, except in very specific cases, there is an ambiguity attached to the definition of meaningful structures in that setting. For this reason, some visualization techniques, most prominently texture-based approaches, have proposed a variety of ad hoc combinations of Eulerian and Lagrangian perspectives in order to overcome the challenge posed by the ambiguity of patterns that is both coherent in space and time.

In this paper we leverage a concept called *Finite-Time Lyapunov Exponent* (FTLE) that has its roots in dynamical systems theory and has been recently

introduced in the fluid dynamics community to resolve this ambiguity. To that end we propose to combine the visual effectiveness of texture-based representations with the physically intuitive meaning of the coherent Lagrangian structures characterized by FTLE. Our method leverages the performance of the Graphics Processing Unit (GPU) to accelerate pre-computation of FTLE and to create expressive animations of the flow that the user can interactively adjust to fit the needs of his visual analysis. We present the application of this approach to the visualization of three different transient flows obtained through Direct Navier-Stokes simulations. While the use of a GPU implementation results in a significant speed-up of the FTLE computation, interactive speeds are still out of reach. For this reason, and due to limitation of space, we wish to concentrate on visualization aspects in the following and do not discuss the technical details of a GPU implementation.

The paper is structured as follows. We first provide a brief introduction to the notion of FTLE. We then discuss some related work in the fluid dynamics and the visualization literature. Section 4 describes and justifies the visualization methods we use while section 5 shows the results obtained for three Computational Fluid Dynamics (CFD) data sets. Finally, we conclude our presentation with a discussion of the benefits and current limitations of our method and we point out interesting avenues for future work.

## 2 The Finite-Time Lyapunov Exponent

The *finite-time Lyapunov exponent* (FTLE) is a geometric tool that can be used to define and extract coherent structures in transient flows studied in a Lagrangian framework. It has been the object of a growing interest in fluid dynamics research over the last few years and has been successfully applied to a variety of fluid dynamics problems. The Lyapunov exponent is in fact a basic theoretical notion used in the analysis of dynamical systems where it permits to characterize the rate of separation of infinitesimally close trajectories. Its application to aperiodic time-dependent flows, however, has been only recently proposed by Haller [6]. We introduce in the following the basic concepts that are necessary to understand the steps involved in the FTLE computation as we apply them in section 5. As such our presentation is voluntarily informal and we refer the interested reader to the publications listed in section 3 for a more in-depth treatment of this rich subject.

We start by introducing some notations. We consider a time-dependent two-dimensional vector field  $\mathbf{v}$  defined over a finite Euclidean domain  $U \subset \mathbb{R}^2$  and a (typically finite) temporal domain  $I \subset \mathbb{R}$ . The position  $\mathbf{x}$  of a particle starting at position  $\mathbf{x}_0$  at time  $t_0$  after advection along the resulting flow is therefore a function  $\mathbf{x}(t, t_0, \mathbf{x}_0)$  satisfying  $\mathbf{x}(t_0, t_0, \mathbf{x}_0) = \mathbf{x}_0$  and  $\frac{\partial \mathbf{x}}{\partial t} \Big|_{\tau} = \mathbf{v}(\tau, \mathbf{x})$ . The basic idea behind the notion of FTLE is to define asymp-

totically stable and unstable coherent structures in terms of loci of maximized dispersion of closely seeded particles. Specifically, consider a fixed initial time  $t_0$  and a fixed time interval  $\tau$ , defining  $t = t_0 + \tau$ . A linearization of the local variations of the map  $\mathbf{x}(t, t_0, \cdot)$  around the seed position  $\mathbf{x}_0$  is obtained by considering its spatial gradient  $J_{\mathbf{x}}(t, t_0, \mathbf{x}_0) := \nabla_{\mathbf{x}_0} \mathbf{x}(t, t_0, \mathbf{x}_0)$  at  $\mathbf{x}_0$ . We can now use this gradient to determine the dispersion after time  $\tau$  of particle seeded around  $\mathbf{x}_0$  at time  $t_0$  as a function of the direction  $\mathbf{d}_{t_0}$  along which we move away from  $\mathbf{x}_0$  at  $t_0$ :  $\mathbf{d}_t = J_{\mathbf{x}}(t, t_0, \mathbf{x}_0) \mathbf{d}_{t_0}$ . Maximizing the norm  $|\mathbf{d}_t|$  over all possible unit vector directions  $\mathbf{d}_{t_0}$  corresponds to computing the norm of  $J_{\mathbf{x}}(t, t_0, \mathbf{x}_0)$  according to the matrix norm  $\|\mathbf{A}\| := \max_{|\mathbf{x}|=1} |\mathbf{A}\mathbf{x}|$ . This norm is known to be the square root of the maximal eigenvalue  $\lambda_{\max}$  of the positive definite matrix  $\mathbf{A}^T \mathbf{A}$ . Therefore maximizing the dispersion of particles around  $\mathbf{x}_0$  at  $t_0$  over the space of possible directions around  $\mathbf{x}_0$  is equivalent to computing  $\sqrt{\lambda_{\max}(J_{\mathbf{x}}(t, t_0, \mathbf{x}_0)^T J_{\mathbf{x}}(t, t_0, \mathbf{x}_0))}$ . This quantity is directly related to the *largest finite-time Lyapunov exponent*  $\Lambda(t, t_0, \mathbf{x}_0) = \log(\lambda_{\max}(J_{\mathbf{x}}(t, t_0, \mathbf{x}_0)^T J_{\mathbf{x}}(t, t_0, \mathbf{x}_0))^{\frac{1}{2}(t-t_0)})$ .

Practically, this quantity can be evaluated for both forward and backward advection. Large FTLE values for forward advection correspond to repelling material lines while large FTLE values for backward advection correspond to attracting material lines. Assuming that the set of seed points correspond to the vertices of a grid (e.g. the computational grid), the map  $\mathbf{x}(t, t_0, \cdot)$  can be evaluated by numerical integration of pathlines along the flow and its spatial gradient can then be computed with respect to the underlying seeding grid. As noted in [6] the proper identification of attracting and repelling material lines requires to extract ridges from the FTLE field. Ridges of a scalar field  $\alpha$  correspond to loci where  $\nabla \alpha$  is orthogonal to the minor eigenvector of the Hessian matrix  $\nabla^2 \alpha$ , under the assumption that the corresponding minor eigenvalue is negative [1]. Observe that the solution proposed in [12] based on the integration of particles along the gradient field of FTLE constitutes in fact an approximation of an actual ridge line computation that is prone to errors. Moreover it has performed poorly in our test cases, due in part to the noise inherently present in our estimates of the FTLE gradient. For these reasons we chose to present in our results the values of FTLE without extracting the corresponding ridges. We show in section 5 that a proper color map is able to emphasize those ridges without explicit extraction of their geometry.

### 3 Previous Work

As we mentioned previously, Haller has pioneered the use of FTLE as a means to characterize coherent Lagrangian structures in transient flows [6]. In his seminal paper he presented this approach as a geometric one, in contrast to another analytic criterion that he proposed simultaneously based on the

notion of preservation of a certain stability type of the velocity gradient along the path of a particle. This work followed previous papers by the same author investigating similar criteria derived from the eigenvectors of the Jacobian of the flow velocity along pathlines to determine the location of Lagrangian coherent structures in the two-dimensional setting [3, 4].

This initial research has generated in the fluid dynamics community a significant interest in FTLE and its applications to the structural analysis of transient flows, both from a theoretical and from a practical viewpoint. Haller proposed a study of the robustness of the coherent structures characterized by FTLE under approximation errors in the velocity field [7]. In the same paper, he suggests to identify attracting and repelling material lines with ridge lines of the FTLE field. Shadden et al. provided a formal discussion of the theory of FTLE and Lagrangian coherent structure [13]. One major contribution of their paper was to offer an estimate of the flow across the ridge lines of FTLE and to show that it is small and typically negligible. An extension of FTLE to arbitrary dimensions is discussed in [10]. These tools have been applied to the study of turbulent flows [5, 2, 12]. They were used in the analysis of vortex ring flows [14]. These notions were also applied to a control problem [8].

On the visualization side of things, multiple approaches have been explored to permit the extraction and the effective depiction of the structures exhibited by time-dependent flows. Topological methods have been applied to transient flows in the Eulerian perspective [18, 16, 17]. Theisel et al. also proposed a method to characterize the structure of pathlines by subdividing the domain into sink, source, and saddle-like regions based on the divergence of the restriction of the flow to a plane orthogonal to the pathline orientation in space-time [17].

Additionally, texture-based representations have been considered to visualize time-dependent flows while offering an effective depiction of salient structures, see [9] and references therein. Because of the intrinsic difficulty of defining structures that are both coherent in space and time, each of these methods resorts to some form of ad hoc way to combine the Eulerian and Lagrangian perspectives, leading to animations for which a physical interpretation is typically ambiguous.

In the present work we therefore propose to combine a texture-based representation method called *GPUFLIC* that we introduced recently [11] with a visual encoding of FTLE in order to emphasize meaningful patterns in a common flow visualization modality and to clarify their relationship with coherent Lagrangian structures.

## 4 Visualization of Coherent Structures

In this section, we show how a direct visualization of the FTLE field for a given flow can be achieved. While the direct numerical computation of the FTLE for a dense sampling of a given flow region with adequate resolution is usually prohibitively expensive, we were able to reduce computation times significantly by employing the computational power available through the use of commodity graphics hardware (GPU). We will not give our method here, due to space considerations, but will present it in forthcoming work. Instead, we will focus on visualization of the results of this computation.

### 4.1 Direct FTLE Visualization

The earliest work on direct FTLE visualization was again done by Haller [6], who used a dense color mapping to visualize basic FTLE structures that covers all primary colors. With this approach, Lagrangian coherent structures appear as local maximizing lines of the FTLE field. However, his visualization is unfortunate in the sense that maximizing lines are not intuitively identifiable with a single color. If weaker coherent structures exist, they may have a different color than the stronger structures elsewhere in the field. Therefore, this technique does not lend itself well to an intuitive understanding. One possible remedy for this is a ridge extraction followed by the visualization of these locally maximizing lines. However, these approaches are usually highly sensitive to numerical issues, and can result in false positives. Moreover, coherent structures are presented in a skeletonized fashion, clearly describing their existence but not the relative strength.

A second topic of importance is the temporal orientation of the FTLE computation. Looking at the FTLE in forward time, it is essentially a measure of the maximal stretching of pathlines, and is therefore a good candidate to visualize coherent structures of a diverging nature. To achieve similar results for converging structures, it is necessary to also look at the FTLE in backward time, i.e. compute the measure of pathline convergence. In the following, we will abbreviate these two different scalar measures  $\text{FTLE}^+$  and  $\text{FTLE}^-$  to indicate forward resp. backward temporal orientation. Again, naive color mapping has difficulties of representing these two quantities for incompressible flows, since they often show regions of saddle-type behavior where both  $\text{FTLE}^+$  and  $\text{FTLE}^-$  have a significant value together, simply because they do not follow an exclusive-or relationship.

We therefore propose a two-dimensional color mapping scheme. First, we normalize the FTLE fields over the space-time domain of the given dataset to the unit interval, using the same normalization on both fields in order to preserve the relative strength of coherent structures. Then, we apply the two-dimensional colormap presented in Fig. 4, resulting in a visualization that represents converging structures in blue and diverging structures in red, encoding the relative strength through saturation. Figure 1 provides an example. We

will discuss how this enables an analysis of typical flow patterns from FTLE visualizations in more detail in Section 5.

Although geometric context can be provided through explicit depiction of domain boundaries and objects embedded in the flow, a more flow-centric context is often needed to interpret FTLE visualizations in terms of flow mechanics. In the next section, we will briefly discuss a simple yet intuitive approach which, in combination with direct FTLE visualization, can provide insightful visualizations.

## 4.2 GPUFLIC

*GPUFLIC* [11] is the texture-based flow visualization method that we use in conjunction with FTLE to depict the evolution of salient structures in the transient flows introduced in the next section. This method constitutes an efficient implementation on the GPU of an algorithm proposed by Shen and Kao called UFLIC [15]. The basic idea of this scheme consists in advecting a dense set of particles that deposit the color attribute that they carry as they traverse the space time domain. At each instant in time, each pixel of the texture covering the domain averages the contributions made by all the particles that crossed it during the last time step, which creates a frame of the animation. Additionally, to maintain a good contrast as the animation progresses, a high-pass filtering step is applied to each frame and combined with an input noise to produce the color attributes assigned to a whole new set of particles – one per pixel – that are injected into the flow at each time step. Refer to [11] for a more detailed description of the algorithm.

## 4.3 In-context FTLE Visualization

To provide the necessary context for FTLE visualization, we propose a simple combination of the FTLE and GPUFLIC flow visualizations. By multiplicatively weighting the color channels in the images generated by both methods for the same domain (with the same integration parameters), we obtain more expressive visualizations (see e.g. Fig. 1). This is essentially facilitated by the dense nature of GPUFLIC in contrast to the sparse representation typically obtained with FTLE in the presence of clearly defined structures. Where GPUFLIC expresses the basic Lagrangian information such as flow direction and magnitude, FTLE complements this nicely with information about coherence and convergence.

A slightly different visualization effect is achieved by encoding FTLE information into a single scalar field, based on the balance of convergence and divergence of pathlines. Since, in the total absence of either, the flow is uniform, these properties can be augmented with an interpretation in terms of forcing the flow into certain patterns: at a point of high divergence, the flow is forced away from this point. The opposite is true for points of high convergence. A good analogy is the gradient field of a scalar height field. Therefore,

by encoding the balance between  $\text{FTLE}^+$  and  $\text{FTLE}^-$  in a scalar field, we draw on a natural physical understanding of height fields and their gradients. Again, the resulting visualization is enhanced with the FTLE and GPUFLIC results as texture. Fig. 6 demonstrates this.

Having discussed several possible techniques to apply the FTLE for direct visualization of two-dimensional flow fields, we move on to specific datasets and the visualization results obtained there using these methods.

## 5 Results

All specific visualization examples described in this section center on results obtained from CFD datasets. They are adaptive-resolution, time-adaptive unsteady direct numerical simulations of the incompressible Navier-Stokes equations. Three basic types of flow were chosen because each of them lends itself well to illustrate different aspects of FTLE-based visualization. We only treat the first dataset in detail and, due to space limitations, only present basic results for the other two.

### 5.1 Kármán Vortex Street

The Kármán Vortex Street is one of the most widely known patterns in fluid mechanics. It consists of a vortex street behind a cylinder and is a special case of unsteady flow separation from bluff bodies embedded in the flow. It is quite well understood and therefore an ideal test case for many applications.

Figure 1 illustrates the basic modes of direct unsteady flow visualization presented in this work. The top image shows only the direct FTLE color map. It identifies the separation structures behind the cylinder (red) that separate the region of vortex genesis directly behind the cylinder from the surrounding flow. The curved attachment structures (blue) visualize the convergence of material at the vortices. As the flow moves away from the cylinder, these structures are essentially advected and grow weaker. We observe that for a ridge-line type visualization (without encoding of feature strength), the weakening of structures would not be observable. The combination of FTLE and GPUFLIC (bottom image of Fig. 1) allows for a visual identification of individual vortical structures. Since they are necessarily counterrotating, FTLE depicts the boundaries as line-type divergent regions. GPUFLIC alone does not achieve an identification of structures except close to the cylinder (middle image) and is only comprehensible if enhanced by FTLE visualization (Fig. 6).

We further employ this well-understood example to study some of the properties of the Finite-Time Lyapunov Exponent. Figure 5 shows the effect of different integration lengths on the FTLE computation. As a general rule, coherent structures become more pronounced with increasing integration time, as pointed out in [12]. On the other hand, long integration (in comparison to the reference time, in other words the natural time scale of the problem) may

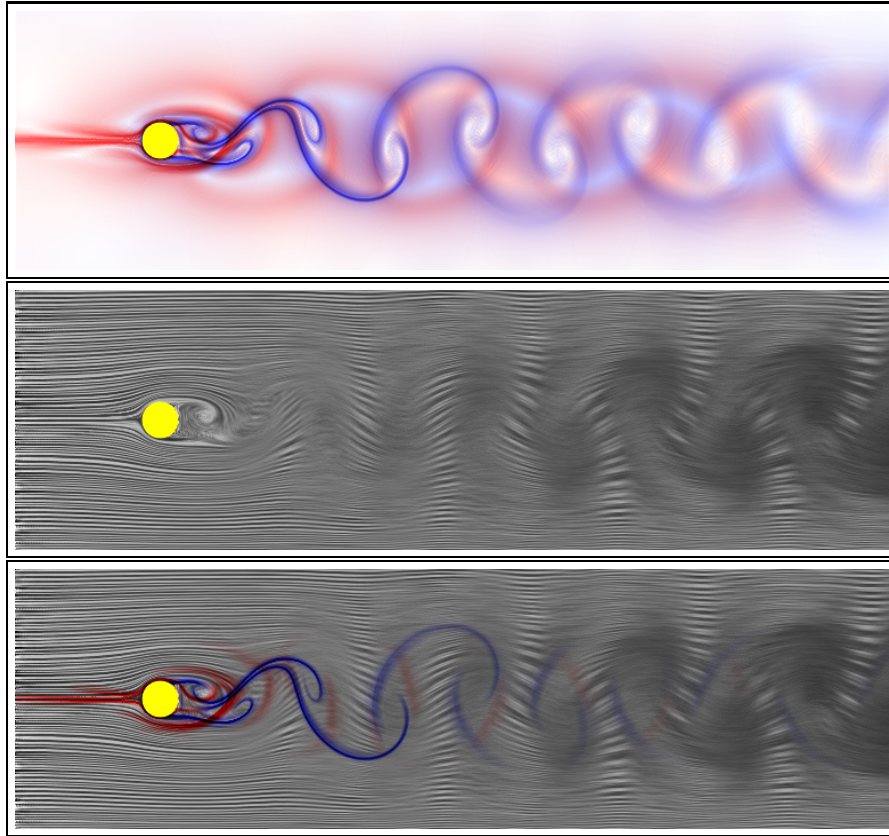


**Fig. 1.** Comparison: Direct FTLE visualization (**top**), UFLIC (**middle**), a combination of both (**bottom**).

yield coherent structures that are not actually meaningful for short-term flow evolution, see [7]. We conclude from this that the reference time, which can be interpreted as a measure for the rate of change of the flow field, seems like a good choice for the integration length.

A related topic is the application of FTLE visualization to stationary flow fields. If the integration length is (theoretically) increased to infinity in such fields, the local maximum lines of the resulting coherent structures should coincide with the topological graph of the flow field. Figure 2 illustrates the resulting features (top image) in comparison to the unsteady results (bottom image). Behind the cylinder, the structures are very topological in nature, i.e. they are attracting and repelling material lines intersecting at saddle-like points. However, the vortical characterization is lost as the flow is advected (topology is not Galilean invariant), and the flow pattern is unclear. Over-

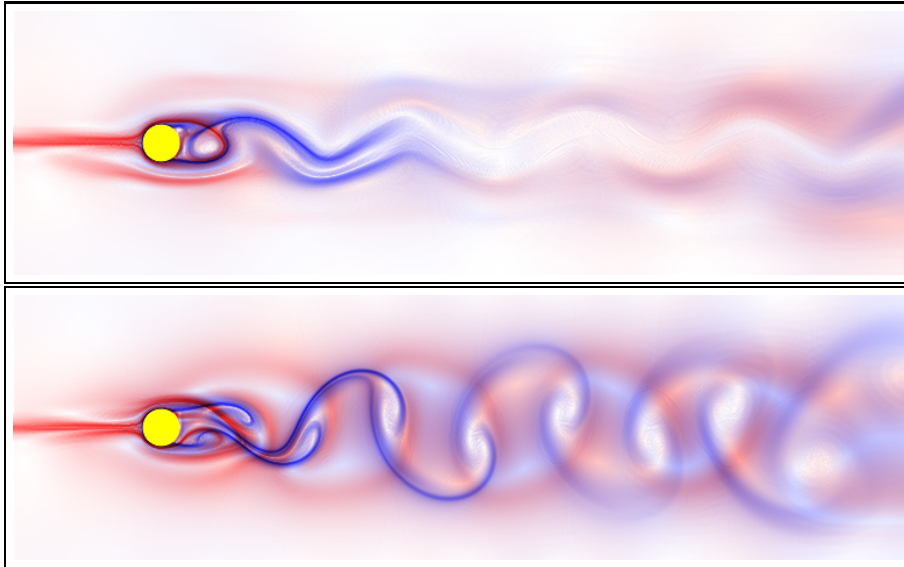


**Fig. 2.** Comparison: Direct FTLE visualization, steady case (**top**), unsteady case (**bottom**).

all, these results suggest that FTLE-type analysis is a possible adaptation of topological methods to unsteady flows.

## 5.2 Heated Cylinder Flow

This example was computed using the classical Boussinesq approximation to simulate the flow generated by a heated cylinder. This approximation adds a source term proportional to the temperature (modeled as a diffusive material property) to the vertical component of the velocity field. The cylinder serves as a temperature source and thereby generates a *plume* of upward flowing material. As the plume moves upward, its outer layers exchange heat with the surrounding flow, resulting in inhomogeneous friction and hence turbulent flow. Figure 7 shows four timesteps of the resulting visualization using the proposed methods. The interpretation here is more difficult than for the previous dataset since there is more structure on smaller scales, and hence more detail. Quite evident, however, is the clear separation of plume-related flow from the overall surrounding flow.

## 5.3 Rayleigh-Taylor instability

The term “Rayleigh-Taylor instability” essentially refers to the interactions of two fluids of different density. In this example, we have chosen an initial

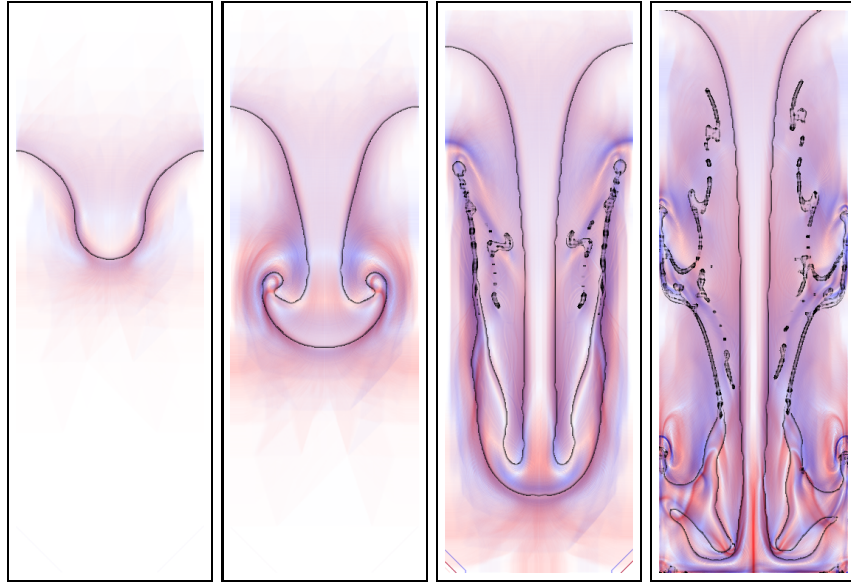


**Fig. 3.** Direct FTLE visualization for the Rayleigh-Taylor instability, context is provided by the boundary between the two fluids.

configuration in which a denser fluid rests on top of a lighter fluid. As the simulation progresses, the upper fluid is drawn downwards by gravity, resulting in the typical (inverse) mushroom structure. This flow differs from the already presented examples in several respects.

First, the time resolution is limited by the appearance of small-scale structures at the material interface whose temporal evolution must be correctly resolved. The resulting GPUFLIC visualization is unsatisfying due to the strong variation of scales that makes it difficult to choose an integration time that will equally accentuate all relevant structures. Therefore, to provide context to the FTLE visualization, we have added the material interface to the resulting images (Figure 3, black lines). This provides enough orientation to make results comprehensible.

The second difference to the previous examples is the relative weakness and large extent of coherent structures. While one would expect the material interface to show up clearly in the FTLE images, this is not the case. Enlarging the integration time to provide for more coherent structures is ruled out by the range of the simulation, since clearly it is not possible to integrate pathlines past the end of the simulation. We conclude that this flow contains only few long-term coherent structures and is mainly driven by small-scale motion. In comparison to the previous examples, FTLE values are an order of magnitude smaller, which is obscured in visualization by the normalization we apply (see 4).

## 6 Discussion

In this paper, we have empirically studied the Finite Time Lyapunov Exponent and its applications in the visualization of time-dependent planar flows. We have shown how the visualization can be greatly enhanced by an explicit choice of color mapping and a combination with the GPUFLIC technique. Furthermore, we have taken first steps to examine various aspects of the FTLE such as dependence on integration time and application to steady flows. These aspects were illustrated on three typical examples of unsteady, two-dimensional flows.

Future work seems promising and manifold: While we were able to produce good visualization results for the test cases, we would like to study application examples, where the FTLE can possibly help in solving some of the more difficult problems in flow analysis, like the extraction of separation and attachment lines on curve surfaces. As a general theme, a generalization of the presented concepts and algorithms to higher dimensions seems necessary to study unsteady volume flows.

### Acknowledgements

Parts of this work were financially supported by DFG and the International Research Training Group (IRTG) at the University of Kaiserslautern.

We would especially like to thank Gordon Kindlmann for making his TEEM software publically available. It has proven very helpful in the process of developing the visualizations presented here.

### References

1. D. Eberly, R. Gardner, B. Morse, and S. Pizer. Ridges for image analysis. *Journal of Mathematical Imaging and Vision*, 4:355–371, 1994.
2. M.A. Green, C.W. Rowley, and G. Haller. Detection of lagrangian coherent structures in 3d turbulence. *J. Fluid Mech.*, to appear, 2006.
3. G. Haller. Finding finite-time invariant manifolds in two-dimensional velocity fields. *Chaos*, 10(1):99–108, 2000.
4. G. Haller and G. Yuan. Lagrangian coherent structures and mixing in two-dimensional turbulence. *Physica D*, 147:352–370, 2000.
5. G. Haller. Lagrangian structures and the rate of strain in a partition of two-dimensional turbulence. *Physics of Fluids*, 13(11), 2001.
6. G. Haller. Distinguished material surfaces and coherent structures in three-dimensional flows. *Physica D*, 149:248–277, 2001.
7. G. Haller. Lagrangian coherent structures from approximate velocity data. *Physics of Fluids*, 14(6):1851–1861, june 2002.
8. T. Inanc, S.C. Shadden, and J.E. Marsden. Optimal trajectory generation in ocean flows. In *Proceedings of the American Control Conference*, pages 674–679, 2005.

9. B. Laramée, J.J. van Wijk, B. Jobard, and H. Hauser. ISA and IBFVS: Image space based visualization of flow on surfaces. *IEEE Transactions on Visualization and Computer Graphics*, 10(6):637–648, nov 2004.
10. F. Lekien, S.C. Shadden, and J.E. Marsden. Lagrangian coherent structures in n-dimensional systems. *Physica D*, submitted, 2006.
11. G.-S. Li, X. Tricoche, and C.D. Hansen. GPUFLIC: Interactive and dense visualization of unsteady flows. In *Data Analysis 2006: Proceedings of Joint IEEE VGTC and EG Symposium on Visualization (EuroVis) 2006*, pages 29–34, may 2006.
12. M. Mathur, G. Haller, T. Peacock, J.E. Ruppert-Felsot, and H.L. Swinney. Uncovering the lagrangian skeleton of turbulence. *Phys. Rev. Lett.*, submitted, 2006.
13. S.C. Shadden, F. Lekien, and J.E. Marsden. Definition and properties of lagrangian coherent structures from finite-time lyapunov exponents in two-dimensional aperiodic flows. *Physica D*, 212:271–304, 2005.
14. S.C. Shadden, J.O. Dabiri, and J.E. Marsden. Lagrangian analysis of fluid transport in empirical vortex ring flows. *Physics of Fluids*, 18:047105, 2006.
15. H.W. Shen and D.L. Kao. A new line integral convolution algorithm for visualizing unsteady flows. *IEEE Transactions on Visualization and Computer Graphics*, 4(2), 1998.
16. H. Theisel and H.-P. Seidel. Feature flow fields. In *Proceedings of Joint Eurographics - IEEE TCVC Symposium on Visualization (VisSym '03)*, pages 141–148, 2003.
17. H. Theisel, T. Weinkauff, H.-C. Hege, and H.-P. Seidel. Topological methods for 2d time-dependent vector fields based on streamlines and path lines. *IEEE Transactions on Visualization and Computer Graphics*, 11(4):383–394, 2005.
18. X. Tricoche, T. Wischgoll, G. Scheuermann, and H. Hagen. Topology tracking for the visualization of time-dependent two-dimensional flows. *Computer and Graphics*, 26:249–257, 2002.

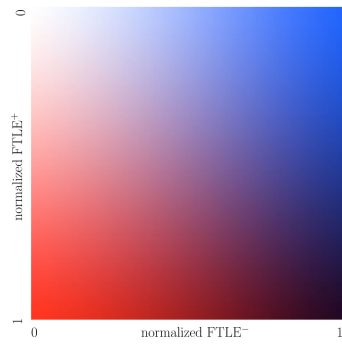


**Fig. 4.** Colormap.

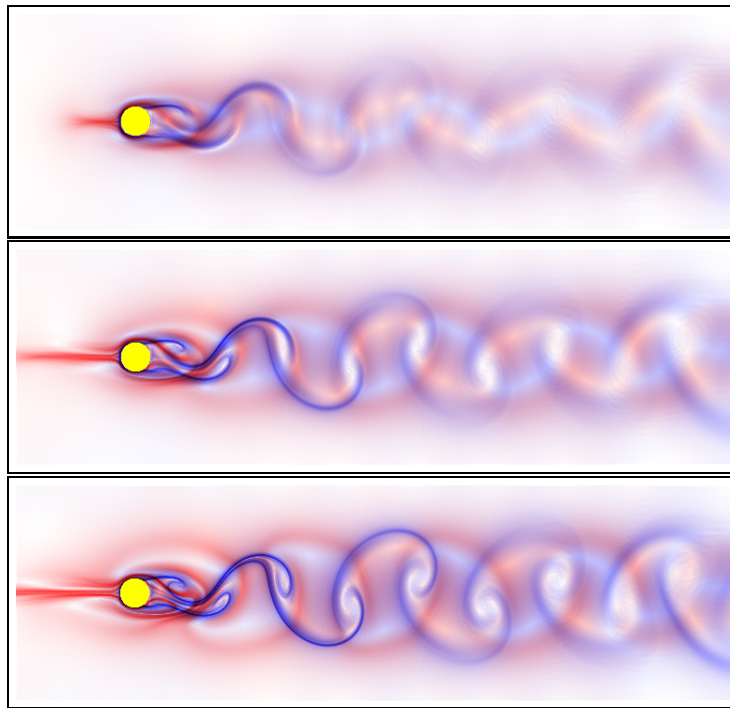


**Fig. 5.** Comparison: Direct FTLE visualization, different integration times. 0.25 (top), 0.5 (middle), 0.75 (bottom).

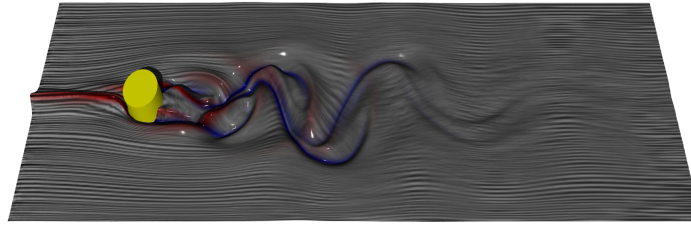


**Fig. 6.** Height field visualization of FTLE with UFLIC texture and FTLE color coding.

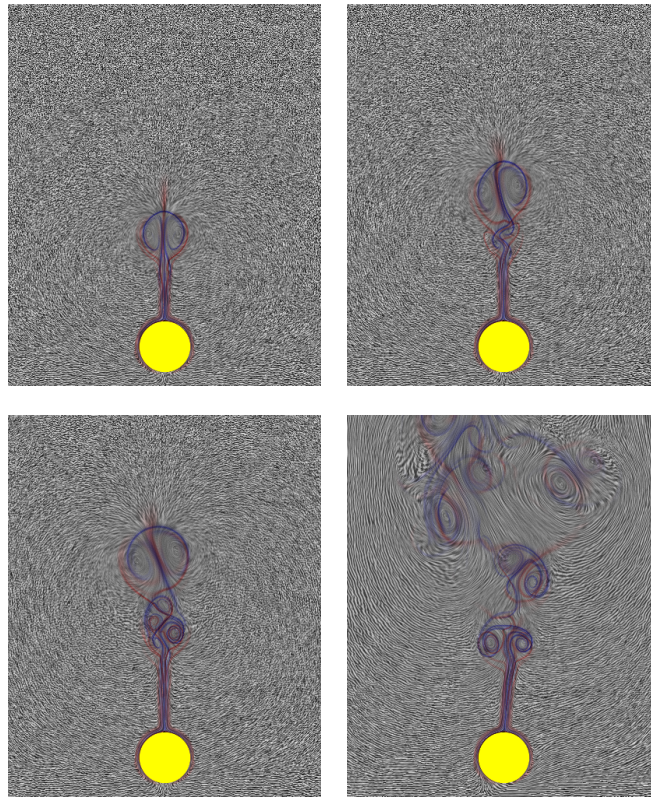


**Fig. 7.** Comparison: Direct FTLE visualization (**middle**), UFLIC (**top**), a combination of both (**bottom**).